Biomedical Optics EXPRESS

STED imaging of green fluorescent nanodiamonds containing nitrogen-vacancy-nitrogen centers

Gregoire Laporte[1,*] and Demetri Psaltis[1]

[1]*Laboratory of Optics, School of Engineering, École Polytechnique Fédérale de Lausanne (EPFL), Station 17, 1015 Lausanne, Switzerland*

[*]*gregoire.laporte@epfl.ch*

Abstract: We report Stimulated Emission Depletion (STED) imaging of green fluorescent nanodiamonds containing Nitrogen-Vacancy-Nitrogen (NVN) centers with a resolution of 70 nm using a commercial microscope. Nanodiamonds have been demonstrated to have the potential to be excellent cellular biomarkers thanks to their low toxicity and nonbleaching fluorescence, and are especially appealing for superresolution imaging technique like STED microscopy. However, only red fluorescent nanodiamonds containing Nitrogen-Vacancy (NV) centers have been used with STED microscopy so far. The existence of only one color nonbleaching center limits the possible observations, for instance it complicates spatial correlation studies with STED. To provide a nonbleaching probe in a different color, we characterize here the optical properties of the NVN defect for STED imaging. We demonstrate STED imaging of the green fluorescent nanodiamonds containing NVN centers, opening the door for long term two-color STED observation. Furthermore we exemplify the use of green nanodiamonds as a second color nonbleaching STED biomarker by imaging 70 nm fluorescent crystals up taken into HeLa cells.

OCIS codes: (170.2520) Fluorescence microscopy; (100.6640) Superresolution; (160.4236) Nanomaterials; (160.2220) Defect-center materials.

References and links

1. K. I. Willig, B. Harke, R. Medda, and S. W. Hell, "STED microscopy with continuous wave beams," Nat. Methods **4**(11), 915–918 (2007).
2. E. Rittweger, K. Y. Han, S. E. Irvine, C. Eggeling, and S. W. Hell, "STED microscopy reveals crystal colour centres with nanometric resolution," Nat. Photonics **3**(3), 144–147 (2009).
3. K. Y. Han, K. I. Willig, E. Rittweger, F. Jelezko, C. Eggeling, and S. W. Hell, "Three-dimensional stimulated emission depletion microscopy of nitrogen-vacancy centers in diamond using continuous-wave light," Nano Lett. **9**(9), 3323–3329 (2009).
4. K. I. Willig, S. O. Rizzoli, V. Westphal, R. Jahn, and S. W. Hell, "STED microscopy reveals that synaptotagmin remains clustered after synaptic vesicle exocytosis," Nature **440**(7086), 935–939 (2006).
5. N. D. Halemani, I. Bethani, S. O. Rizzoli, and T. Lang, "Structure and Dynamics of a Two-Helix SNARE Complex in Live Cells," Traffic **11**(3), 394–404 (2010).
6. S.-J. Yu, M.-W. Kang, H.-C. Chang, K.-M. Chen, and Y.-C. Yu, "Bright fluorescent nanodiamonds: no photobleaching and low cytotoxicity," J. Am. Chem. Soc. **127**(50), 17604–17605 (2005).
7. J. Tisler, G. Balasubramanian, B. Naydenov, R. Kolesov, B. Grotz, R. Reuter, J.-P. Boudou, P. A. Curmi, M. Sennour, A. Thorel, M. Börsch, K. Aulenbacher, R. Erdmann, P. R. Hemmer, F. Jelezko, and J. Wrachtrup, "Fluorescence and spin properties of defects in single digit nanodiamonds," ACS Nano **3**(7), 1959–1965 (2009).
8. Y. Kuo, T.-Y. Hsu, Y.-C. Wu, and H.-C. Chang, "Fluorescent nanodiamond as a probe for the intercellular transport of proteins in vivo," Biomaterials **34**(33), 8352–8360 (2013).
9. T.-J. Wu, Y.-K. Tzeng, W.-W. Chang, C.-A. Cheng, Y. Kuo, C.-H. Chien, H.-C. Chang, and J. Yu, "Tracking the engraftment and regenerative capabilities of transplanted lung stem cells using fluorescent nanodiamonds," Nat. Nanotechnol. **8**(9), 682–689 (2013).

#251122 Received 8 Oct 2015; revised 19 Nov 2015; accepted 30 Nov 2015; published 7 Dec 2015

10. T.-C. Hsu, K.-K. Liu, H.-C. Chang, E. Hwang, and J.-I. Chao, "Labeling of neuronal differentiation and neuron cells with biocompatible fluorescent nanodiamonds," Sci. Rep. **4**, 5004 (2014).
11. A. M. Zaitsev, "Vibronic spectra of impurity-related optical centers in diamond," Phys. Rev. B **61**(19), 12909–12922 (2000).
12. R. Heintzmann and M. G. L. Gustafsson, "Subdiffraction resolution in continuous samples," Nat. Photonics **3**(7), 362–364 (2009).
13. M. Mission, M. F. Rate, and V. M. Model, "Measuring two key parameters of H3 color centers in diamond," NASA Tech Briefs. **25**, 24–25 (2005).
14. T.-L. Wee, Y.-W. Mau, C.-Y. Fang, H.-L. Hsu, C.-C. Han, and H.-C. Chang, "Preparation and characterization of green fluorescent nanodiamonds for biological applications," Diamond Related Materials **18**(2-3), 567–573 (2009).
15. S. C. Rand and L. G. Deshazer, "Visible color-center laser in diamond," Opt. Lett. **10**(10), 481–483 (1985).
16. Y. Kuo, T.-Y. Hsu, Y.-C. Wu, J.-H. Hsu, and H.-C. Chang, "Fluorescence lifetime imaging microscopy of nanodiamonds in vivo," in *SPIE OPTO* (International Society for Optics and Photonics, 2013), pp. 863503–863503–7.
17. B. R. Smith, D. Gruber, and T. Plakhotnik, "The effects of surface oxidation on luminescence of nano diamonds," Diamond Related Materials **19**(4), 314–318 (2010).
18. J.-H. Hsu, W.-D. Su, K.-L. Yang, Y.-K. Tzeng, and H.-C. Chang, "Nonblinking green emission from single H3 color centers in nanodiamonds," Appl. Phys. Lett. **98**(19), 193116 (2011).
19. E. Rittweger, B. Rankin, V. Westphal, and S. Hell, "Fluorescence depletion mechanisms in super-resolving STED microscopy," Chem. Phys. Lett. **442**(4-6), 483–487 (2007).
20. K. I. Willig, B. Harke, R. Medda, and S. W. Hell, "STED microscopy with continuous wave beams," Nat. Methods **4**(11), 915–918 (2007).
21. L.-J. Su, C.-Y. Fang, Y.-T. Chang, K.-M. Chen, Y.-C. Yu, J.-H. Hsu, and H.-C. Chang, "Creation of high density ensembles of nitrogen-vacancy centers in nitrogen-rich type Ib nanodiamonds," Nanotechnology **24**(31), 315702 (2013).
22. Y. K. Tzeng, O. Faklaris, B. M. Chang, Y. Kuo, J. H. Hsu, and H. C. Chang, "Superresolution imaging of albumin-conjugated fluorescent nanodiamonds in cells by stimulated emission depletion," Angew. Chem. Int. Ed. Engl. **50**(10), 2262–2265 (2011).
23. O. Faklaris, D. Garrot, V. Joshi, F. Druon, J.-P. Boudou, T. Sauvage, P. Georges, P. A. Curmi, and F. Treussart, "Detection of single photoluminescent diamond nanoparticles in cells and study of the internalization pathway," Small **4**(12), 2236–2239 (2008).
24. O. Faklaris, D. Garrot, V. Joshi, J. P. Boudou, T. Sauvage, P. Curmi, and F. Treussart, "Comparison of photoluminescence properties of semiconductor quantum dots and non-blinking diamond nanoparticles and observation of the diffusion of diamond nanoparticles in cells," J. Eur. Opt. Soc Rapid Publ. **4**, 09035 (2009).
25. E. Neu, D. Steinmetz, J. Riedrich-Möller, S. Gsell, M. Fischer, M. Schreck, and C. Becher, "Single photon emission from silicon-vacancy colour centres in chemical vapour deposition nano-diamonds on iridium," New J. Phys. **13**(2), 025012 (2011).
26. J. Humpolícková, A. Benda, and J. Enderlein, "Optical saturation as a versatile tool to enhance resolution in confocal microscopy," Biophys. J. **97**(9), 2623–2629 (2009).

1. Introduction

STED microscopy is a superresolution imaging technique that has revolutionized optical microscopy in the last two decades. It results in breaking the diffraction limit of a fluorescence laser scanning microscope by depleting the fluorescence around the focus by stimulated emission. STED microscopy offers a resolution well below the diffraction limit [1,2], in the three dimensions [3], and it has been used to tackle many problems in biology [4,5]. However, the requirement of high power to obtain efficient depletion accelerates photobleaching and severely limits the observation time. One solution is to develop dyes and fluorescent probes with less photobleaching. In this sense color centers in diamond have an exceptional property: they do not exhibit photobleaching and are exceptionally photostable [6]. They are therefore excellent luminescent sources for far field fluorescence nanoscopy by STED, and NV centers have been imaged in many STED microscopy studies [2,3,7]. Furthermore, nanodiamonds are highly biocompatible and have been used as bioimaging agents. They have been used for instance to probe intercellular transport of yolk protein [8], but also as intracellular probe to track the lung stem cell regeneration [9] and to label the neuronal differentiation [10].

Diamond hosts more than 500 different luminescent centers [11], emitting from the deep-ultraviolet (UV) to the far infrared (IR). However, so far only NV center emitting red fluorescence were subject to superresolution techniques. Other color centers have been

#251122 Received 8 Oct 2015; revised 19 Nov 2015; accepted 30 Nov 2015; published 7 Dec 2015

largely unexplored for superresolution imaging and their properties relevant to STED imaging is of great interest. We present here STED superresolution imaging of nanodiamonds with NVN defects that exhibit green fluorescence. We analyze the luminescence characteristics of the NVN centers in nanocrystals and relate them to stimulated emission properties. By comparing with the properties of NV centers extensively studied in the literature, we show that the NVN center is an excellent candidate for STED nanoscopy. We measured a resolution of 70 nm which is the specified limit of our system. The excellent photo-stability under the STED observation we report here should allow for higher resolution with optimized laser system [2]. Finally, in order to show the potential of green nanodiamonds (gNDs) as photostable biomarkers in fluorescence nanoscopy, we acquired superresolved images of 70 nm sized diamond particles uptaken into HeLa cells.

2. Stimulated emission characteristics

Superresolution imaging techniques often rely on a nonlinear relationship between the excitation intensity and the fluorophores response [12]. In the case of STED microscopy, the saturation of the emission depletion is employed. The extent of this saturation determines the degree to which the effective PSF can be narrowed. In other words, the STED microscopy performance is directly related to the photophysical properties of the fluorescent probes. So, in order to estimate their applicability to STED microscopy, we characterize here the fluorescence properties of NVN center in nanodiamonds.

2.1 Absorption and emission spectra

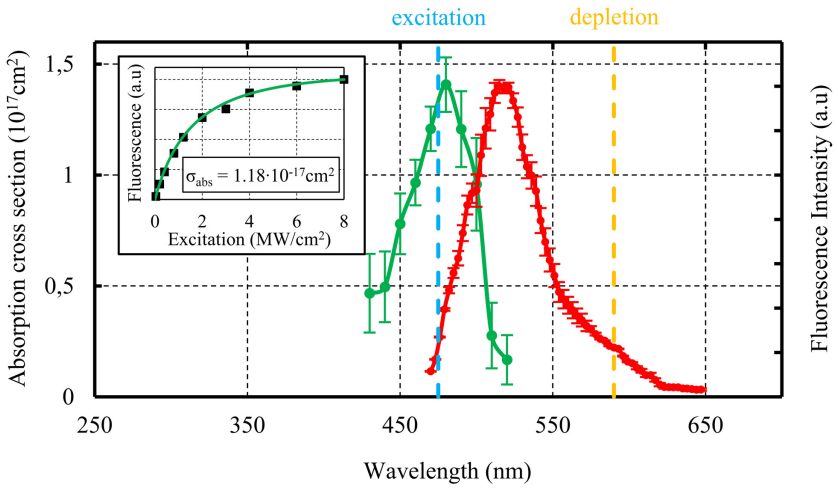

Fig. 1. Absorption (green plot) and emission (red plot) spectra of green nanodiamonds. The absorption spectrum is deduced from the measurement of the luminescence saturation for each excitation wavelength. The inset displays one example of saturation curve at 470 nm excitation. For this nanodiamond, the fitting of the curve results in an absorption cross section of $1.18 \cdot 10^{-17}$ cm^2 (more details in Appendix A). Each point of the absorption curve is the average value over 16 gNDs and the standard deviation is indicated with error bars. The emission luminescence spectrum is measured by varying the detection window for a fixed 458 nm excitation wavelength. The emission spectrum shows a large tail at 600 nm. Each point of the emission curve is the average value over 30 gNDs and the standard deviation is indicated with error bars. The two vertical color lines indicate the wavelengths of the excitation and depletion beams used for the superresolution imaging.

The neutral NVN center is composed of one vacancy next to two substitutional nitrogen atoms in the diamond lattice. The 70 nm gNDs were ordered from Adamas-Nanotechnologies and dried at a 0.01 mg.mL^{-1} on a glass slide for photophysical properties characterization.

#251122 Received 8 Oct 2015; revised 19 Nov 2015; accepted 30 Nov 2015; published 7 Dec 2015

The sparsity of the prepared sample at such a concentration was checked by scanning electron microscopy (Appendix B). Thus, the fluorescent recorded is predominantly emitted by single nanocrystals. Figure 1 displays the absorption and emission spectra of the nanodiamonds containing NVN color centers. As suggested in [13], the absorption spectrum was derived independently from the number of defects from the saturation intensity measurement for each excitation wavelength (Inset in Fig. 1, more details in the Appendix A). The maximum absorption cross section at the peak is found to be $1.4 \cdot 10^{-17}$ cm^2 which is slightly lower than previous measurement [14]. It can be observed in Fig. 1 that variability among individual particles and the uncertainty on the curve fitting lead to significant error bars on the absorption spectrum measurement. However, in good agreement with previous reports, the absorption spectrum exhibits a clear peak around 480 nm.

The emission spectrum was measured directly onto the confocal STED microscope for a fixed excitation wavelength at 458 nm and changing the detection spectral window with an acousto-optic tunable filter. It can be observed in Fig. 1 that the excitation of the NVN centers results in a broad fluorescence emission between 500 and 600 nm with a peak at about 530 nm [14]. The stokes shift is larger than typical organic dye like Atto routinely used for STED imaging. This large stokes shift eliminates any absorption of the depletion light. Moreover, the wide emission spectrum leads to keep a significant stimulated emission cross section at the depletion wavelength of 590 nm.

2.2 Fluorescence lifetime

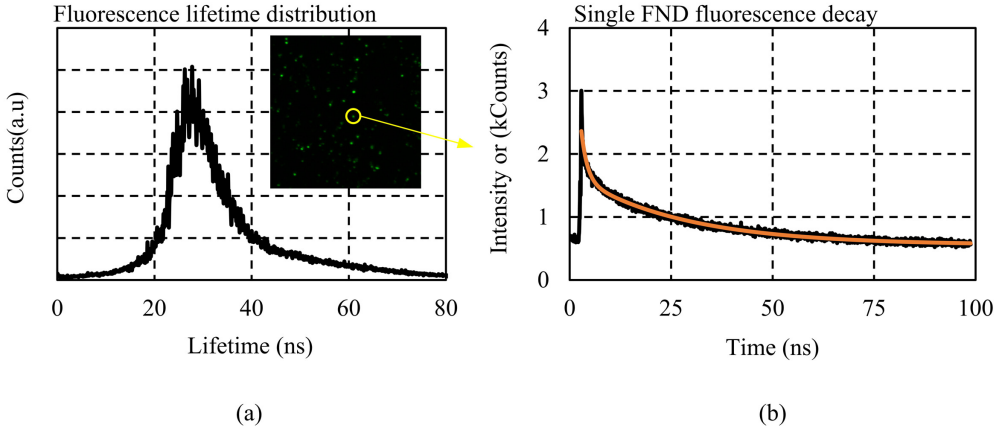

Fig. 2. (a) Fluorescence lifetime distribution of gNDs immobilized on a glass slide (the inset shows the fluorescence image of the gNDs). (b) Fluorescence decay trace of a single nanodiamond situated into the yellow circle in the inset image. The best fit (red curve) is obtained with a two-exponential model.

A separated fluorescence lifetime imaging (FLIM) system was used to obtain lifetime-resolved images of gNDs (picosecond pulsed laser LDH-P-C-440 B (Picoquant), Module PicoHarp 300 (PicoQuant) on SP8 microscope (Leica)). In order to obtain the fluorescence lifetime distribution over a large number of particles we performed fluorescence lifetime imaging on gNDs dispersed on a glass slide (inset in Fig. 2(a)). As presented in Fig. 2(a), we obtained a mean value of $\tau = 27$ ns and a full width half maximum (FWHM) of 10.1 ns. The lifetime value is significantly larger than in the bulk one (16 ns) [15] and is also larger than the red fluorescent nanodiamonds (rNDs) [3]. The large dispersion has already been observed with rNDs. It has been explained by the change in the conformation of the particle (cluster or single particle) inducing variation in the refractive index around each particle and also by the different dipole orientation of the emitters at the glass-air interface [7].

#251122 Received 8 Oct 2015; revised 19 Nov 2015; accepted 30 Nov 2015; published 7 Dec 2015

In order to characterize the nature of the defect contained in the gNDs, we also extracted the fluorescence decay trace for each nanodiamond with the same FLIM system. One example is presented in Fig. 2(b). All the fluorescence time traces recorded exhibit double-exponential decays with a fast component (τ<3 ns) and a slow component ($\tau \approx 27$ ns). This double-exponential decay has been previously observed in rNDs [3,16,17]. The major slow component is characteristic from the luminescence of the NVN center and the fast component is attributed to surface effects [17].

2.3 Stimulated emission cross section

The basis of the STED microscopy is to deplete the fluorescence signal by stimulated emission. The stimulated emission properties of NVN centers has been studied previously in macroscopic crystals for the production of a color center laser in diamonds. Laser action at 530 nm has been observed, confirming the potential use of NVN color center with stimulated emission [15]. However, as we described in the lifetime measurement, in nanocrystals smaller than the excitation wavelength, the emission properties can be modified. The radiative transition in NVN crystal has been shown to occur with a high quantum yield of 0.95 [18]. Knowing the fluorescence decay time and the quantum yield of the transition, the stimulated emission cross section can be derived from the emission spectrum measurement [19]: $\sigma_s = \frac{\lambda^4 E(\lambda)}{(8\pi \cdot c \cdot n^2)}$, where λ is the wavelength, E is the fluorescence intensity normalized to the quantum yield ($\int E(\lambda)\, d\lambda = 0.95$), c the speed of light and n the refractive index of the material. For different wavelengths, the result is displayed in the Fig. 3(b). At the wavelength used here for STED imaging (590 nm), we find $\sigma_s \approx 0.45 \cdot 10^{-17}$ cm^2.

The theoretical prediction is confirmed by measuring the depletion of the luminescence as a function of the STED beam power. In continuous STED, both the excitation beam and the depletion beam are on, so the excited state is constantly populated while the luminescence emission competes with the stimulated emission process. The luminescence rate is given by the inverse of the luminescence lifetime ($1/\tau_f$) while the stimulated emission rate is equal to ($\sigma_s I_{exc} \lambda / (hc)$) and scales with the excitation intensity (I_{exc}). Under the assumption that the excitation saturation is low, the depletion intensity required to switch off half of luminescence signal is $I_s = hc / (\sigma_s \lambda \tau_f)$ and the depletion curve is described by a function of the form $1/(1 + I_{sted}/I_s)$ [20]. The luminescence inhibition curve presented in Fig. 3(a) is an average over 18 measurements, taken from different individual nanodiamonds particles. As seen from the error bars, all individual curves are a bit different from each other's. This is a logical consequence of the luminescence decay time inhomogeneity mentioned in the previous paragraph. From the curve in Fig. 3(a), the cross section of luminescence inhibition is found to be $\sigma_s \approx 0.49 \cdot 10^{-17}$ cm^2 in good agreement with the value determined from the emission spectrum. The consistency in between the two values confirms that the mechanism for fluorescence quenching is stimulated emission.

#251122 Received 8 Oct 2015; revised 19 Nov 2015; accepted 30 Nov 2015; published 7 Dec 2015

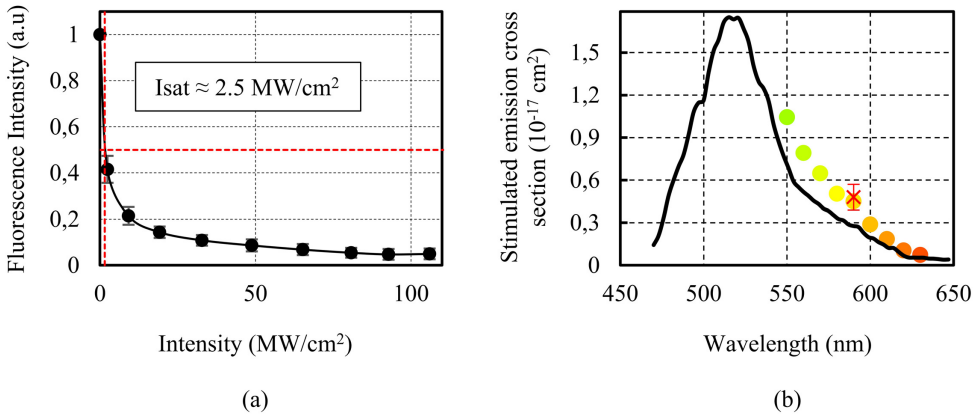

Fig. 3. (a) Fluorescence inhibition curve of single gND as a function of the depletion CW beam intensity. The depletion intensity necessary to switch-off half of the luminescence characterizes the steepness of the curve and is directly related to the stimulated emission cross section. (b) Stimulated emission cross section values in function of the wavelength (color dots) derived from the emission spectrum measurement (black line). The value at 590 nm is in good agreement with the one derived from the depletion curve (red cross).

An ideal emitter for STED microscopy should possess altogether: high quantum yield and photostability, an emission spectra that match the STED wavelength, a long fluorescence lifetime and a low cross-section for multiphoton absorption and for absorption by the excited states. Roughly, gNDs exhibit similar parameters as the rNDs. The stimulated emission cross section of the NVN center is low (Fig. 3(b)) (about one order of magnitude lower than Atto 495 [19]). However, the long luminescence lifetime compensates for the limited emission cross section and results in a steep decrease of the luminescence with the depletion beam intensity (Fig. 3(a)). In addition, in contrast with organic dyes, the gNDs are especially suitable for continuous STED. As the decay time is longer than typical the pulse interval in pulsed mode locked lasers, the average power needed to achieve efficient emission depletion is similar in the continuous STED mode and in the more complex pulsed implementation. Furthermore, with only the depletion beam on, we did not observe any signal from the NDs, which indicates a very limited cross section for multiphoton absorption around 600 nm. We also observed an excellent photostability, which indicates no photochemical alteration of the crystal but also no absorption by the excited states. All those parameters make gNDs well suited for STED nanoscopy.

Although gNDs share the advantages of the rNDs, they also share and even accentuate the main limitation of rNDs, which is the low emission brightness. A small absorption cross section (Fig. 1, about one order of magnitude less than organic dyes) and the very large lifetime (Fig. 2, one order of magnitude longer than organic dyes) result in a dim fluorescence. Indeed, the NVN center absorption cross section is half that of the NV centers [14] (at the absorption peaks), and the radiative lifetime is about 1.5 times longer [3]. So the signal emitted by a NVN center is about 3-times less bright (assuming same quantum yield) than the NV center. In order to overcome this deficiency a large number of color center is needed inside each nanoparticle [21]. We work here with 70 nm commercially available gNDs (Adamas-Nano) specified to contain on average about 60 color centers that should deliver a luminescence intensity equivalent to a few organic dye molecules. Increasing the density of the color centers in nanodiamonds would allow the use of smaller particle as biolabels. Increasing the density of color centers in NDs is an active research area [21].

#251122 Received 8 Oct 2015; revised 19 Nov 2015; accepted 30 Nov 2015; published 7 Dec 2015

3. STED imaging

We have prepared samples composed of 70 nm nanodiamonds containing about 60 NVN centers dried on a glass coverslip. We used a Leica STED-SP5 with 488 nm pulsed excitation and 590 nm CW depletion. In order to obtain the best resolution, high depletion intensity was used (~130 MW/cm^2). As illustrated in Fig. 4(a), the STED image improves the resolution compared to the confocal scan and reveals subwavelength details. The resolution obtained is evaluated by measuring the full width half maximum of a single nanocrystal, we measured the STED resolution to be about 70 nm (measuring a 90 nm FWHM profile in Fig. 4(a) and assuming 50 nm particle, the resolution is even better if the size of the particle is bigger, cf Appendix B), which is consistent with the specification of the machine. Moreover, the green luminescence from the nanodiamonds remains perfectly stable under STED illumination as depicted in Fig. 4(a): after 100 scans, no sign of photobleaching is detected. This excellent photostability is ideal for long-term high resolution observations.

Figure 4(b) illustrates the gNDs properties that can complicate their use as biomarkers. First, they are prone to aggregation. It makes cellular labelling difficult and creates thicker structures that are more difficult to resolve with STED microscope (Fig. 4(b)). So, in order to obtain homogenous [22] or targeted [8] labelling additional surface treatment is required. Second, the number of defect inside gNDs is not homogeneous (Appendix B). So even if the absence of bleaching allows the collection of more photons by increasing the acquisition time to resolve finer details, the brightest particles lead to saturation of the detector. This color center density inhomogeneity is to our opinion the main limitation that needs to be improved for better biological labelling.

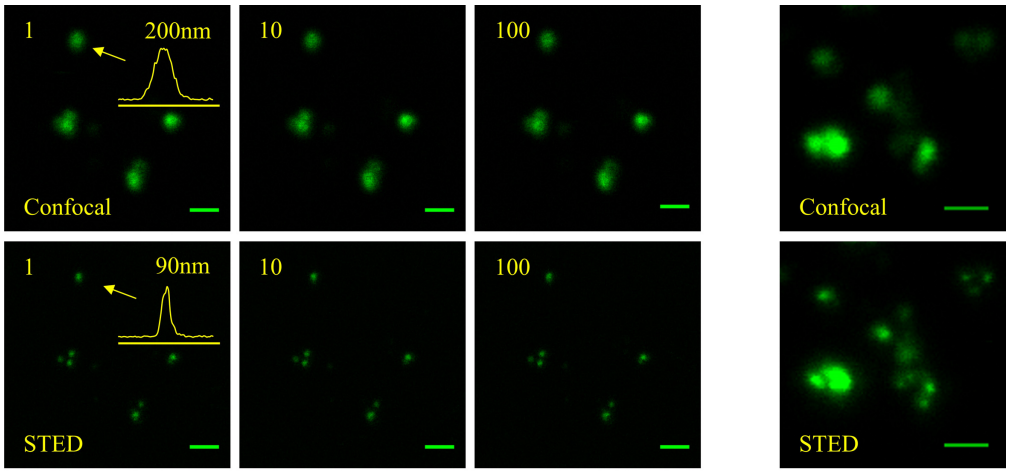

Fig. 4. (a) Consecutive confocal and continuous STED imaging of 70 nm sized nanodiamonds immobilized on a glass slide. The increase in resolution leads to reveal details blurred in the conventional confocal images. The inset on the first images is the profile along the particle indicated with an arrow. It allows for the estimation of the resolution given by STED to be at least 70 nm for a particle bigger than 50 nm (cf. Appendix B). The multiple scans illustrate the perfect photostability. Even if for the STED scan images, high depletion intensity was used (I = 130 MW/cm^2, 256 × 256 pixels with 3 ms dwell time), no change in the recorded signal level is observed after 100 scans. (b) Confocal and STED image revealing the inhomogeneity of the nanoparticles and their tendency to aggregate. Scale bars are 500 nm.

#251122 Received 8 Oct 2015; revised 19 Nov 2015; accepted 30 Nov 2015; published 7 Dec 2015

4. Cell imaging

To investigate if the green nanodiamonds can be imaged better than the diffraction-limited resolution in a biological sample, we demonstrate STED images of gNDs particles inside HeLa cells.

HeLa cells were grown in standard conditions on glass coverslips in Dulbecco's modified eagle medium glutamax medium. The cells were seeded at a density of $8 \cdot 10^4$ cm^{-2} and grown in an incubator at 37 °C for one day. The cells were incubated for 2h with gNDs at a concentration of 10 µg/mL and then incubated for 30min also with WGA Alexa Fluor 680 (life technologies) at 2.5 µg/mL. After incubation, the excess of dye and gNDs was washed three times with phosphate buffer saline solution. The cells were then fixed with 3.5% paraformaldehyde in citrate buffer saline solution and mounted on microscope slides for observation.

The cellular uptake was confirmed with two color confocal imaging. The cell membrane is labelled with the red dye (WGA), proving that the confocal section plane is situated inside the cell (Fig. 5). The nanodiamonds appear on the green fluorescence channel. As in the previous reports [14,23], nanodiamonds tend to form aggregates in the cytoplasm and do not enter the cell nucleus. The presence of green cell autofluorescence is visible in Fig. 5, however the level of the autofluorescence signal is kept low by detecting the fluorescence only 4 ns after the excitation. As the gNDs radiative lifetime is much longer than the autofluorescence decay it improves the signal to background ratio [23]. Some isolated gNDs internalized in the cytoplasm are imaged in the confocal mode and STED mode (Insets in Fig. 5). It can be observed that the SNR is degraded because some part of the fluorescence signal is depleted but enough SNR can be maintained to isolate the single particles that were blurred in the confocal image. We demonstrated here superresolution imaging of gNDs inside fixed cells, however both the STED technique and the nanodiamond probes have been shown to be compatible with live cell imaging [5,8,24].

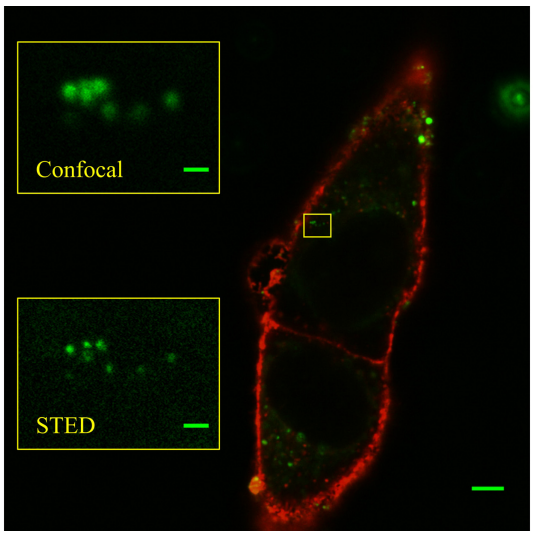

Fig. 5. Superresolution imaging of gNDs up-taken into HeLa cell. The main image is a linear confocal scan. The cell membrane is tagged in red with an organic dye (WGA, Alexa Fluor 680, life technologies), the gNDs appear green and the absence of fluorescence inside the cells reveals the positions of the nuclei. The membrane labelling shows that the confocal section is situated inside the cell and thus it evidences the presence of the nanodiamonds inside the cell. The two insets are magnified images of the highlighted area of the cell. The STED imaging resolves more details about the nanocrystals. Scale bars are 5 µm in the main image and 500 nm in the insets.

#251122 Received 8 Oct 2015; revised 19 Nov 2015; accepted 30 Nov 2015; published 7 Dec 2015

As the rNDs, gNDs, thanks to their high photostability, are useful probes when long acquisition with high resolution is required. In cellular environment they are prone to aggregation, however this can be overcome by surface treatment and specific labelling [8,22]. Owing to their photophysical properties, gNDs are promising candidates as a second color nonbleaching probe for long term nanosensing or nanoimaging application, however two main factors can still be improved for their use as specific marker in superresolved life-science experiment. First, the inhomogeneity of the size of the particle and of the color center density (Appendix B) complicates quantitative studies. Second, the limited density of NVN color center inside the nanocrystals limits the brightness or equivalently the minimal size of particles that can be resolved in cellular environment. Under low excitation intensity, for 10 nm crystals to be as bright as other labels like quantum dots, the color density of our probes should be increased by about two orders of magnitude [21]. Brighter signal can be obtained through higher excitation intensity up to saturation (inset Fig. 1) [24], owing to the gNDs photostability. However, in STED microscopy, excitation works against fluorescence depletion, therefore it implies increasing the STED power accordingly.

5. Conclusion

We have demonstrated that the photophysical properties of gNDs allow their efficient use in STED microscopy. Thanks to their long fluorescence lifetime, gNDs are especially suitable for CW STED implementation. The long lifetime also benefits from time gated detection STED implementation, since the gated detection allows the differentiation of the gND fluorescence from other signals like autofluorescence. However, their long lifetime and low absorption cross section also lead to a low signal brightness. Under our experimental condition, gNDs do not exhibit any photobleaching and despite their limited brightness could still be observed with STED microscopy when internalized into a cell. Because of these characteristics, green nanodiamonds can be used as a second color biocompatible nonbleaching probe for STED microscopy. Many other color centers could be tested to complete the spectrum of the available non bleaching marker for STED nanoscopy, for instance silicon vacancy that exhibit a far red emission [25].

Appendix A: Absorption spectrum measurement

For organic dyes, optical absorption measurement are usually used to determine the absorption cross section. However, the FNDs have a very high refractive index (≈2.4) that induces a lot of scattering and makes the absorption measurement challenging. But also and above all, those methods require the previous knowledge of the number of vacancies in the particle. So, as suggested in [13], we used the fluorescence absorption saturation to derive the absorption spectrum. Indeed, fluorescence saturation is directly related to the light absorbed (no interference of the scattered light) and independent of the number of color center. For fluorescence excitation, we used a white light laser (Fianum SC400) and a tunable filter that can deliver light over the whole visible and IR spectrum (Fig. 6(a)). For each excitation wavelength the fluorescence signal strength is recorded as the excitation power is increased (Inset in Fig. 1). In order to estimate the absorption cross section we consider the simplified model proposed in [26], a two state energy level fluorescent color center (Fig. 6(b)). We also consider a constant approximation rate k_{ex} during the pulse duration (T_p) and a constant fluorescence rate k_f. With those conditions, under steady state condition, the saturation of the fluorescence signal can be shown [26], to be proportional to:

$$I_{fluo} \alpha \frac{k_{ex}}{k_f + k_{ex}} \left(\frac{T_p}{T_{rep}} + \frac{k_{ex}}{T_{rep} k_f (\mathrm{k_f} + \mathrm{k_{ex}})} \left(1 - e^{-(\mathrm{k_f} + \mathrm{k_{ex}}) \mathrm{T_p}} \right) \right) \quad (1)$$

where T_{rep} is the pulse interval. The only unknown in Eq. (1) is the excitation rate during the pulse, which can be expressed in function of the absorption cross section,

#251122 Received 8 Oct 2015; revised 19 Nov 2015; accepted 30 Nov 2015; published 7 Dec 2015

$k_{ex} = \sigma_{abs} I_{exc} T_{rep} / T_p$. Thus, fitting our experimental data with this expression, we can determine the value of σ_{abs} for each wavelength. The excitation power is measured with an optical power-meter (Newport 1830-C), specified with an accuracy of ± 0.4%. This error leads to an accuracy of ± 0.7% on the determined value of σ_{abs} which is well below the precision reported in the error bar in Fig. 1.

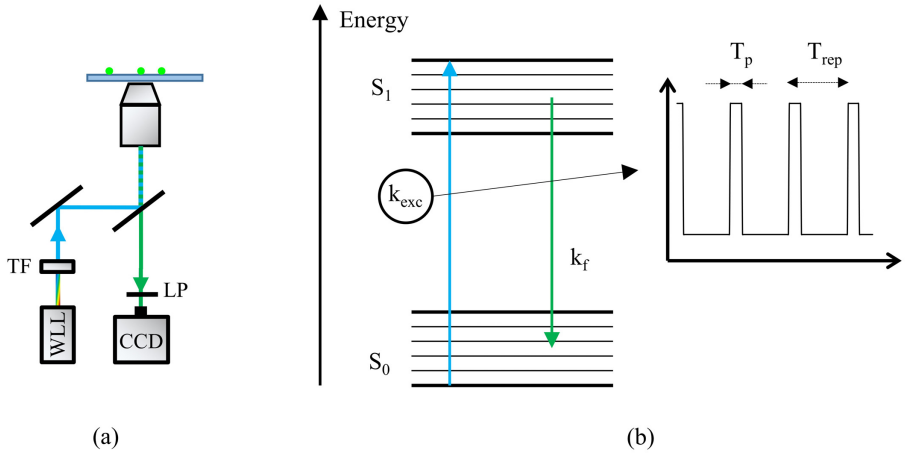

Fig. 6. Absorption spectrum measurement (a) Setup: we use a white light laser (WLL) and a tunable filter (TF) to vary the excitation wavelength. For different excitation intensity and wavelength the fluorescence of the gNDs is filtered out the dichroic mirror (DM) and a long pass filter (LP) and recorded by a CCD. (b) In order to derive the value of the absorption cross section from the fluorescence saturation measurement, we represent the gNDs with two energy levels (the excited state S_1 and the ground state S_0). k_f is the fluorescence rate (we measured the average lifetime (τ_f) in Fig. 2, $k_f = 1/\tau_f$). The WLL is a pulsed source, we assume a constant excitation rate during the pulse, so the excitation rate during the pulse is $k_{ex} = \sigma_{abs} I_{exc} T_{rep} / T_p$.

Appendix B: SEM images of GNDs and particle brightness distribution

The Fig. 7(a) presents a scanning electron microscope image of gNDs dried on a silicon wafer with a concentration of 0.01 $mg.mL^{-1}$. It can be observed that the majority of the particle are isolated. We used the same concentration for our photophysical properties characterization. The Fig. 7(b) shows the size distribution of the particles obtain by analysing a series of similar SEM pictures. The more probable size of the nanocrystals is 70 nm and the nanocrystals are larger than 50 nm. The variations in nanodiamond size and defect density result in a pronounced brightness variability. The Fig. 7(c) shows the brightness distribution of the particles obtained by analysing a series of fluorescent images of dispersed gNDs (prepared with the same concentration).

#251122 Received 8 Oct 2015; revised 19 Nov 2015; accepted 30 Nov 2015; published 7 Dec 2015

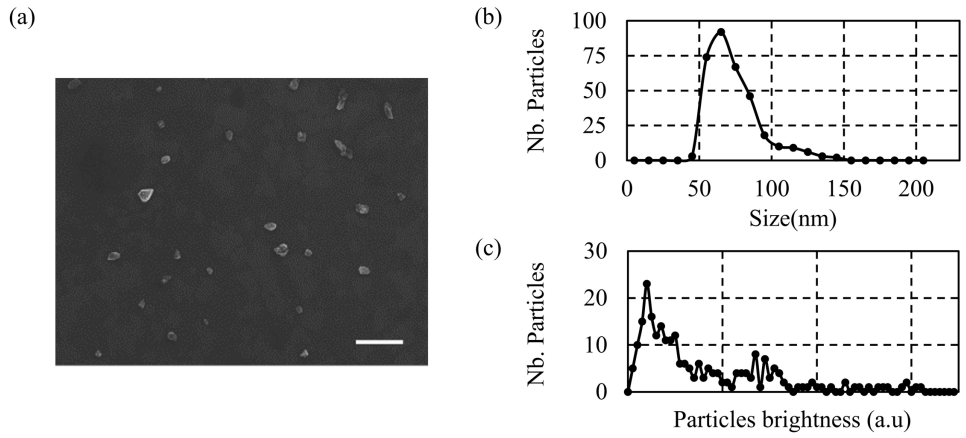

Fig. 7. (a) Scanning electron microscope images of the gNDs. Sparse samples are obtained with gNDs solution of 0.01 mg.mL^{-1}. Scale bar is 500 nm. (b) Size (diameter) distribution of the gNDs. (c) Brightness distribution of the gNDs.

Acknowledgment

We would like to acknowledge all the imaging facility (Biop) team of EPFL, especially Dr. Romain Guiet for the cell preparation and Luigi Bozzo for the fluorescence lifetime measurement. We also would like to acknowledge Dr. Ye Pu for his help with the preparation of the manuscript.